J Mater Sci (2011) 46:7191–7197
DOI 10.1007/s10853-010-4489-1

Synthesis and characterization of chromium spinels as potential electrode support materials for intermediate temperature solid oxide fuel cells

E. Stefan · J. T. S. Irvine

Received: 4 November 2009 / Accepted: 6 April 2010 / Published online: 17 April 2010

Abstract Several spinel compositions, i.e. $Mn_{1+x}Cr_{2-x}O_4$ ($x = 0.7, 0.5, 0$), $MnFe_xCr_{2-x}O_4$ ($x = 0.1, 1$), $MgMnCrO_4$ and $Mg_{1+x}Cr_{2-x}O_4$ ($x = 0, 0.1$) were synthesised and studied in terms of phase analysis, density, stability in reducing atmosphere, electrical conductivity and thermal expansion behaviour. The spinel samples were single phase, with cell parameter values in a good correlation with cation sizes. Most of the studied spinels were found to be unstable under reducing conditions of thermal treatment, except $MnCr_2O_4$, $MgCr_2O_4$ and $Mg_{1.1}Cr_{1.9}O_4$. Electrical properties have been investigated by impedance spectroscopy and DC conductivity measurements at temperatures between 200 and 900 °C.

Introduction

An important challenge for planar solid oxide fuel cells (SOFC) is the development of interconnect materials. The interconnect connects the anode side of one single cell with the cathode side of the adjacent single cell and prevents the fuel and oxidant gas from mixing. SOFC interconnect materials should have high electronic conductivity, good stability in oxidizing and reducing atmospheres and thermal expansion coefficient (TEC) that matches other components of the fuel cell [1].

Ferritic stainless steels are candidate interconnect materials for intermediate temperature SOFC. Chromium-based alloys have some advantages to consider for interconnects, such as compatible coefficient of thermal expansion with the other cell components, low costs and good machinability [2, 3]. The main problem in using these materials for interconnects is their high temperature oxidation. This leads to the formation of oxide scales on interconnect surface. Formed oxide scales contain Cr_2O_3 and due to the high temperatures and water vapours, volatile species containing Cr form and deposit in the electrode pores and at the interface between electrode and electrolyte [4, 5]. This process is known as Cr poisoning of the electrodes. Metallic alloys usually contain Cr, Mn, Fe, Co, Ni and spinels are also formed over the interconnect surface [6].

A large group of 3d-transition metal oxides crystallize in the spinel structure. The family of spinel compounds is represented by the general formula AB_2O_4, where A and B are mainly divalent and trivalent cations, respectively. A cubic close-packed (ccp) lattice is formed by 32 oxygen ions, which forms 64 tetrahedral holes and 32 octahedral holes in one unit cell. One half of the octahedral sites are occupied by B ions and one-eighth of the tetrahedral sites are occupied by A ions. Most spinels have cubic structure and are classified in space group Fd3m [7, 8].

A possibility to avoid the electrode poisoning is the deposition of protective coatings [9]. Spinels have previously been studied as materials for protective coating on interconnect surfaces looking mainly at cobaltite spinels [10, 11]. The electrical properties of a range of other spinel compositions have been reviewed recently [12]. Here, the properties of spinel phases are studied as possible electrode support materials for enhancing steel interconnect compatibility with other components of the fuel cell.

This paper follows from an oral presentation at Hyceltec 2009, the 2nd Iberian Symposium on Hydrogen, Fuel Cells and Advanced Batteries. Guest Editor: Verónica Cortés de Zea Bermudez.

E. Stefan (✉) · J. T. S. Irvine
School of Chemistry, University of St. Andrews, St. Andrews, Fife KY16 9ST, Scotland, UK
e-mail: es487@st-andrews.ac.uk

In the present work, binary and ternary spinels containing chromium, manganese, iron and magnesium were investigated with respect to phase analysis, density, stability in reducing atmosphere, electrical conductivity and thermal expansion behaviour.

Experimental

Sample preparation

Single phase spinel samples with composition $Mn_{1+x}Cr_{2-x}O_4$ ($x = 0.7$, 0.5, 0), $MnFe_xCr_{2-x}O_4$ ($x = 1$, 0.1), $MgMnCrO_4$ and $Mg_{1+x}Cr_{2-x}O_4$ ($x = 0$, 0.1) were prepared using the citric acid–nitrate combustion method. Stoichiometric amounts of $Mn(NO_3)_2{\cdot}4H_2O$ Alfa Aesar (99.98%), $Cr(NO_3)_3{\cdot}9H_2O$ Acros Organics (99%), $Fe(NO_3)_3{\cdot}9H_2O$ Sigma Aldrich(>98%), $Mg(NO_3)_2{\cdot}6H_2O$ Sigma Aldrich (99%) and citric acid ($C_6H_8O_7$) Alfa Aesar(99.5%) were dissolved in distilled water and the solutions were continuously stirred and heated to 300 °C. Usually, an excess of 50% citric acid was added for the certainty of a complete reaction. After the reaction was complete, the obtained powders were calcined at 1,000 °C for 10 h, pressed into pellets (13 mm diameter and 2 ± 0.3 mm thickness) at a pressure of ~200 MPa and sintered at 1,400 °C for 12 h in air.

Structure investigation

X-ray powder diffraction studies were performed using a Philips (PW 1710) X-ray Diffractometer in reflection mode. The obtained diffraction patterns analysis was used to determine the formed crystalline phase(s) and crystal parameters, such as unit cell parameters and theoretical densities.

The morphology of all pellets was studied on a JEOL JSM-5600 Scanning Electron Microscope (SEM). Coating was not necessary, as samples were conductive enough to avoid charging problems.

Stability in reducing atmosphere

In order to test the structural stability of the studied spinel compositions, pellets were sintered in reducing atmosphere, assured by a continuous gas flow of 5% H_2/Ar at 950, 1,000 or 1,050 °C in a tubular furnace, for 20–50 h.

Material properties

Thermal expansion coefficient was determined in air or reducing atmosphere on sintered pellets with 11–13 mm diameter and 2 ± 0.3 mm thickness, using a NETZSCH Dilatometer 402C. Conductivity measurements were performed principally by four-terminal DC measurements and confirmed by impedance spectroscopy from 200 to 900 °C. The impedance data were used to probe the influence of microstructure and were acquired in air. DC electrical conductivity measurements were also recorded for compositions stable in reducing atmosphere assured by a continuous gas flow of 50 cm^3/min 5% H_2/Ar. Four Pt foils of ~1 mm thickness were applied parallel onto a pellet surface with platinum paste and sintered at 900 °C for a good contact between the platinum contacts and the pellet. The areas of electrodes used in impedance were equal to pellets surface areas and were prepared with platinum paste applied on both faces of pellets and sintered at 900 °C.

Results

Stability studies

X-ray diffraction (XRD) results for all studied spinels indicated the existence of one cubic phase. The crystal parameters were determined using STOE Win XPOW software.

Table 1 lists the values for cell parameters and relative densities determined on samples sintered at 1,400 °C in air.

The lattice parameters are in good correlation with the ionic radii of the cations. The decrease of the cell parameter with the decrease of manganese content for spinels $Mn_{1+x}Cr_{2-x}O_4$ can be explained by considering the ionic radius values for Mn^{3+} and Cr^{3+}. $MgCr_2O_4$ shows the smallest cell parameter determined by Mg content on the A-site with a smaller ionic radius than Mn^{2+} or Mn^{3+} [13]. The values of ionic radius of the cations are listed in Table 2.

The stability in reducing atmosphere was tested and spinels $Mn_{1.7}Cr_{1.3}O_4$, $Mn_{1.5}Cr_{1.5}O_4$ and $MgMnCrO_4$ had a similar evolution under reducing conditions. The XRD patterns present extra peaks with respect to the pure phase

Table 1 Determined values for cell parameters and relative densities

Sample	a (Å)	Relative densities (%)
$Mn_{1.7}Cr_{1.3}O_4$	8.4786(3)	70
$Mn_{1.5}Cr_{1.5}O_4$	8.4584(4)	71
$MnCr_2O_4$	8.4394(4)	54
$MnFeCrO_4$	8.4722(16)	93
$MnFe_{0.1}Cr_{1.9}O_4$	8.4462(6)	59
$MgMnCrO_4$	8.3896(8)	70
$MgCr_2O_4$	8.3364(4)	54
$Mg_{1.1}Cr_{1.9}O_4$	8.3389(7)	60

Table 2 Ionic radii of selected cations having various coordination numbers [13]

Cation	Coordination number	Electronic spin	Ionic radius (Å)
Mn^{2+}	IV	HS	0.66
	VI	LS	0.83
		HS	0.67
Mn^{3+}	VI	LS	0.58
		HS	0.65
Cr^{3+}	VI	–	0.615
Fe^{3+}	IV	HS	0.49
	VI	LS	0.55
		HS	0.645
Mg^{2+}	IV	–	0.57
	VI	–	0.72

pattern. The extra peaks correspond to MnO, which is the most probable product to be formed after reducing process.

Samples $MnFeCrO_4$ and $MnFe_{0.1}Cr_{1.9}O_4$ are also unstable in reducing atmosphere, as the XRD analysis reveals. The decomposition of spinel phase takes place forming MnO and metallic Fe as secondary phases. A longer time under reducing atmosphere favours a stronger degradation of spinel. $MnCr_2O_4$ spinel was found to be stable under reducing conditions with no extra peaks observed on the diffraction patterns registered for reduced samples. Also, the composition $MgCr_2O_4$ is stable under reducing conditions and a similar evolution is observed for spinel $Mg_{1.1}Cr_{1.9}O_4$ (Figs. 1, 2, 3).

A cation situated at tetrahedral or octahedral site, coordinated by oxygen anions, will have its electronic configuration influenced by the coordination field that is situated around it. The electron levels of the cation are split, decreasing its energy. The stabilization energy is a function of the electronic configuration of the cation and

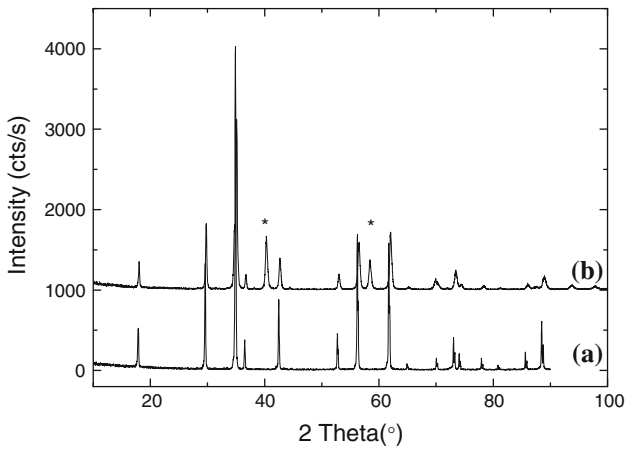

Fig. 1 X-ray diffraction pattern for $Mn_{1.5}Cr_{1.5}O_4$: **a** sintered in air at 1,400 °C; **b** reduced for 20 h at 950 °C; MnO (*asterisk*)

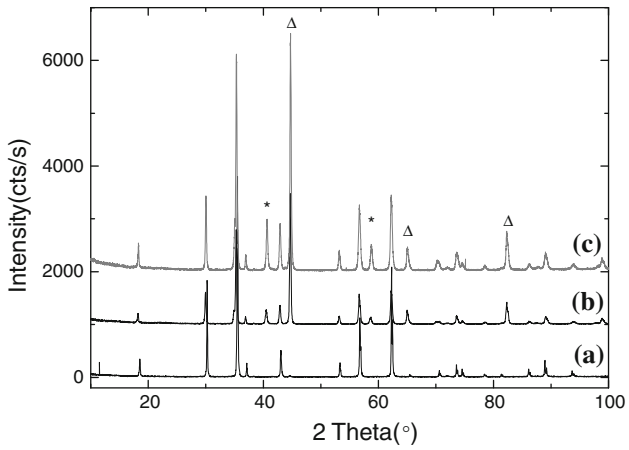

Fig. 2 X-ray diffraction pattern for $MnFeCrO_4$: **a** sintered in air at 1,400 °C for 12 h; **b** reduced at 950 °C for 20 h; **c** reduced at 950 °C for 50 h; MnO (*asterisk*); metallic Fe (*open triangle*)

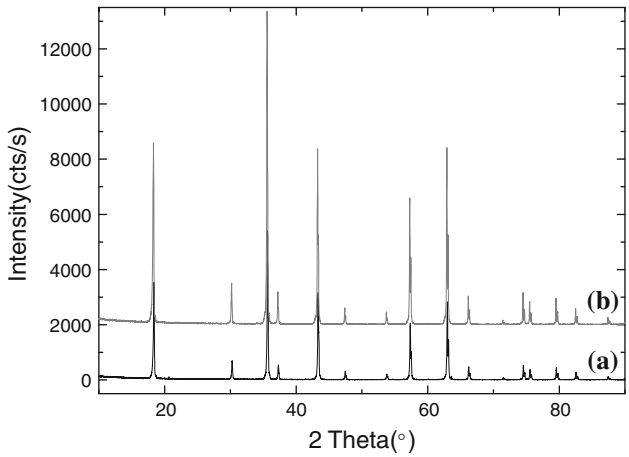

Fig. 3 X-ray diffraction pattern for $MgCr_2O_4$: **a** sintered in air at 1,400 °C for 12 h; **b** reduced at 1,000 °C for 20 h

the coordination polyhedron [8, 14]. In the present work, spinels $MnCr_2O_4$, $MgCr_2O_4$ and $Mg_{1.1}Cr_{1.9}O_4$ were found to be stable under reducing conditions of thermal treatment. The stability of the samples can be explained by the positioning and electronic configuration of the cations that occupy a particular atomic site. Mn^{2+} ($3d^5$, S = 5/2) ions have higher tendency to occupy the tetrahedral sites, while Cr^{3+} ($3d^3$, S = 3/2) ions occupy the octahedral sites, as concluded from thermodynamic data reported by Kovtunenko [8] and from experimental work reported by Yunus et al. [7, 15]. Both ionic configurations are very stable in these atomic sites; therefore, there is no driving force for chemical diffusion and a redistribution of the cations. For Cr^{3+} ($3d^3$, S = 3/2), the triply degenerate t_{2g} orbitals are occupied by three electrons and there is no degree of freedom left at the Cr site [14]. Also cations Mg^{2+} [Ne] have stable electronic configuration at

tetrahedral sites and they have the possibility to occupy octahedral sites also (see composition $Mg_{1.1}Cr_{1.9}O_4$).

Samples with compositions $Mn_{1.7}Cr_{1.3}O_4$, $Mn_{1.5}Cr_{1.5}O_4$, $MnFeCrO_4$ and $MnMgCrO_4$ have similar morphology, high porosity and the particles have different sizes, generally a bi-modal distribution of particles could be defined and there are no strong signs of densification.

For composition MnFeCrO4, the difference between the sizes of the particles is more pronounced, the dimensions for the bigger particles are 10–50 μm, while the small particles have dimensions of ~1–5 μm, while for MgMn CrO_4 the difference between the particle dimensions is the smallest with dimensions of 10–15 and 1–5 μm. $MnCr_2O_4$ presents particles of 0.5–8 μm, $MgCr_2O_4$ from ~0.1 to 3 μm and $Mg_{1.1}Cr_{1.9}O_4$ from ~0.5 to 5 μm. Figure 4 presents the SEM images for most of discussed compositions.

Compatibility with yttrium stabilized zirconia

In order to evaluate the structural and chemical compatibility of studied materials with yttrium stabilized zirconia (YSZ), a series of experiments were performed. Structural compatibility of the two phases was evaluated by comparing the values of TEC (K^{-1}) of the spinel with the YSZ TEC ($10.5 \cdot 10^{-6}$ K^{-1}) [16] (Table 3).

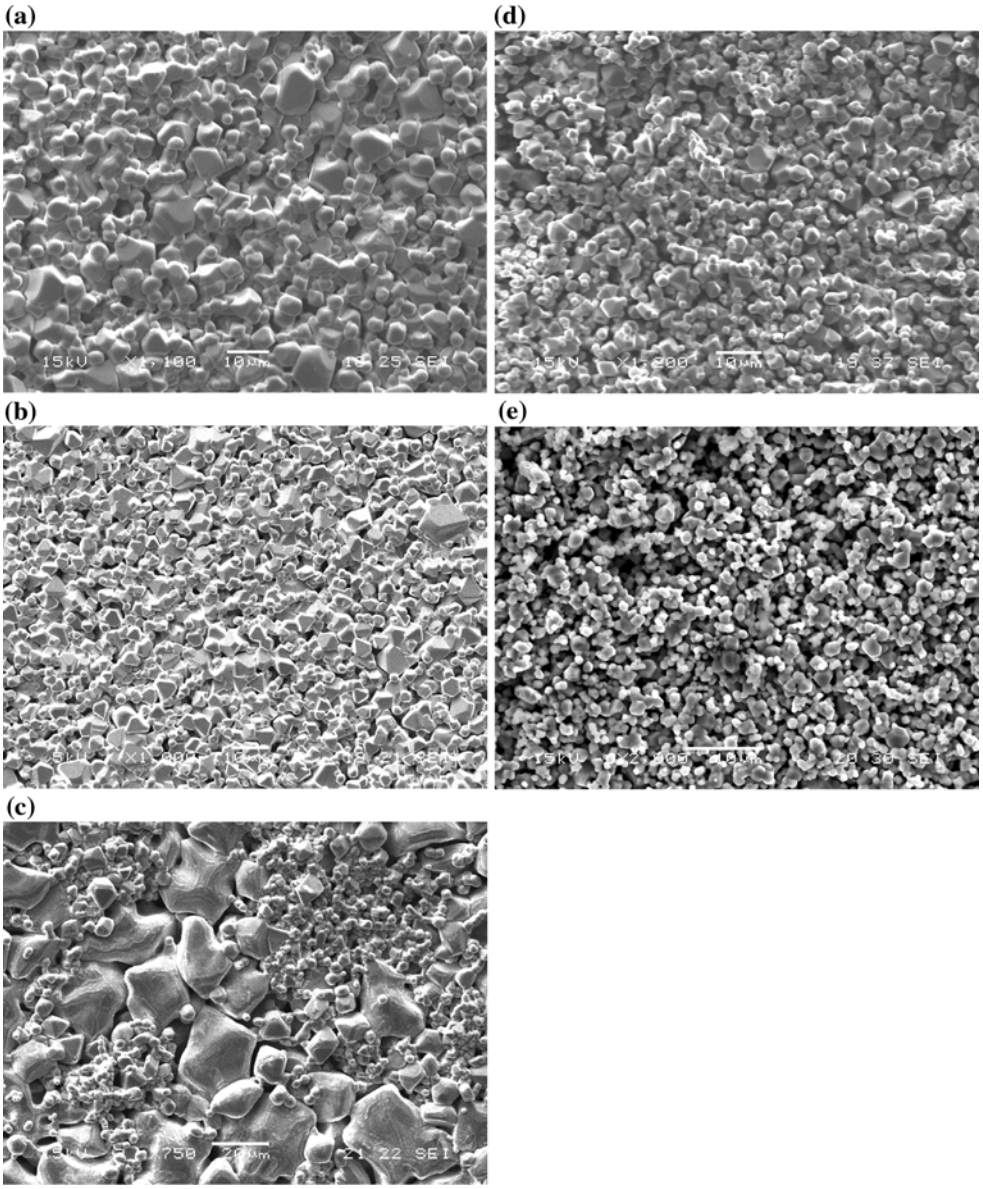

Fig. 4 SEM images acquired on samples sintered at 1,400 °C: **a** $Mn_{1.5}Cr_{1.5}O_4$; **b** $MgMnCrO_4$; **c** $MnFeCrO_4$; **d** $MnCr_2O_4$; **e** $MgCr_2O_4$

Table 3 Thermal expansion coefficients between 100 and 900 °C

Material	TEC (10^{-6} K^{-1})	
	Air	5% H_2/Ar
$MnCr_2O_4$	7.47	7.06
$MgMnCrO_4$	9.61	–
$MgCr_2O_4$	6.08	8.42
$Mg_{1.1}Cr_{1.9}O_4$	8.14	10.04
$MnFeCrO_4$	9.93	–
$MnFe_{0.1}Cr_{1.9}O_4$	9.57	–

Compositions stable to reduction have a poorer expansion match with YSZ compared to the ones that decompose, except $Mg_{1.1}Cr_{1.9}O_4$, which presents good TEC values with respect to YSZ TEC value.

The relative densities of tested specimens are given in Table 1 and they correspond to considered application, as electrode support materials.

The chemical compatibility with YSZ was tested by forming a mixture of spinel and YSZ (8 mol.%) with ratio 1:1, mixed by manual grinding and then milled for 1.5 h using acetone as milling solvent. The obtained powder was pressed into pellets and fired at 1,400 °C for 10 h. XRD and SEM analysis proved the presence of the two phases, spinel and YSZ with no other extra phases. The chemical compatibility was tested for compositions $MgMnCrO_4$ and $Mg_{1+x}Cr_{2-x}O_4$ ($x = 0$, 0.1). XRD pattern and SEM image acquired for spinel $Mg_{1.1}Cr_{1.9}O_4$ are shown in Fig. 5.

Electrical measurements

DC electrical measurements were recorded in order to determine the conductivity versus temperature (from 200 to 900 °C). Figure 6 shows the Arrhenius plots of electrical conductivities measured in air for $Mn_{1.5}Cr_{1.5}O_4$, $MnCr_2O_4$ and $MnFe_{0.1}Cr_{1.9}O_4$. Linear dependences were obtained in the temperature range ~200–900 °C.

Each composition presents two linear regions with a slight change of slope of the Arrhenius plot, which indicates the existence of two conduction mechanisms along the temperature range.

$Mn_{1.5}Cr_{1.5}O_4$ shows a change of slope at ~370 °C with activation energy values of 0.813 and 0.556 eV above and below this temperature. For $MnFe_{0.1}Cr_{1.9}O_4$, the slope change appears at ~605 °C. The corresponding activation energies are 1.168 eV above 605 °C and 0.837 eV below this temperature; $MnCr_2O_4$ changes activation energy at ~590 °C, from 0.602 to 0.860 eV.

The total conductivity of $Mn_{1.5}Cr_{1.5}O_4$ is about one order of magnitude higher than the conductivity of $MnCr_2O_4$ at 900 °C. Lu and Zhu [17] reported that for a wider range of x in the compounds $Mn_{1+x}Cr_{2-x}O_4$

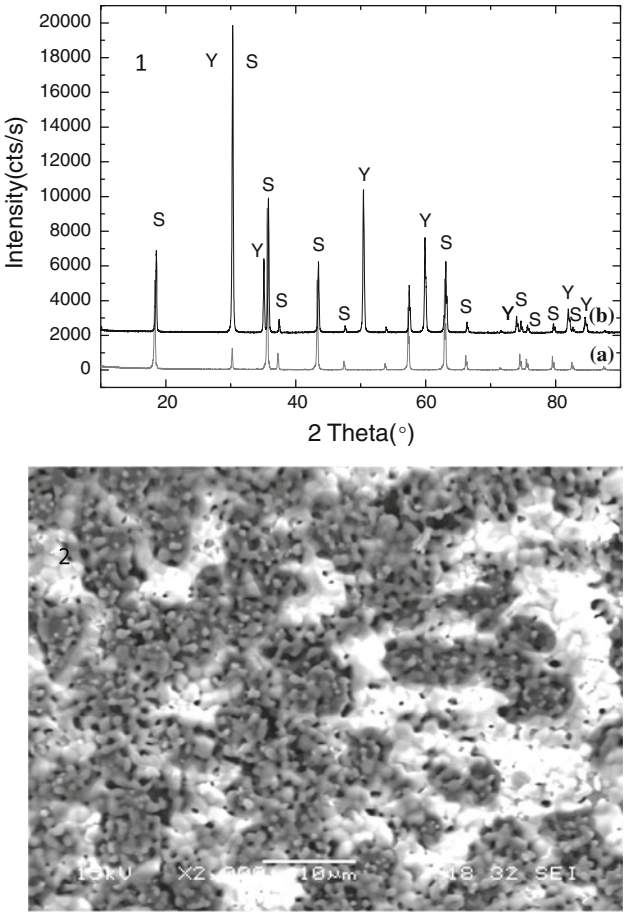

Fig. 5 Chemical compatibility of $Mg_{1.1}Cr_{1.9}O_4$ with YSZ: **1** X-ray diffraction patterns for *a* $Mg_{1.1}Cr_{1.9}O_4$ sintered at 1,400 °C for 12 h; *b* mixture $Mg_{1.1}Cr_{1.9}O_4$:YSZ (8 mol.%) sintered at 1,400 °C for 10 h; S—spinel; Y—YSZ (8 mol.%); **2** SEM image for mixture $Mg_{1.1}Cr_{1.9}O_4$:YSZ(8 mol.%) sintered at 1,400 °C for 10 h

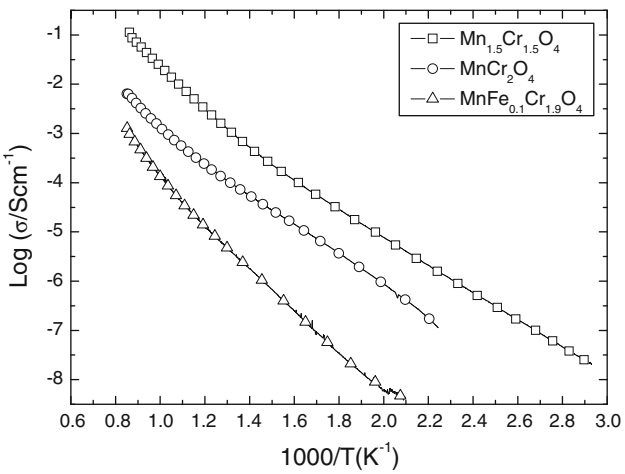

Fig. 6 Temperature dependences of conductivities for $MnFe_{0.1}Cr_{1.9}O_4$, $MnCr_2O_4$, $Mn_{1.5}Cr_{1.5}O_4$ in air for temperature range of 200–900 °C

electronic conductivity increases with the Mn content. A higher content of manganese will facilitate the electronic flow due to the existence of Mn ions with variable valence at B-site in the structure. Conductivity increased with temperature for all studied spinels and confirms the semiconductor behaviour, as reported in literature [18].

AC impedance studies of these Mn:Cr:O spinels showed two components associated with capacitances of order 10^{-12} and 10^{-11} F cm^{-1}. The resistance values obtained from DC four-terminal corresponded well to the resistance values associated with capacitance 10^{-12} F cm^{-1} [19], which would be expected to arise from the bulk or grain component. It, therefore, seems that the 10^{-11} F cm^{-1} element arises from a surface layer as it is not apparent in four-terminal measurements. This surface component was much more apparent when Pt was used as electrode than when Au was used. It is thought to arise from the reduction of the spinel surface by organics as has previously been observed [20], although it might alternatively arise from a potential mismatch between the semiconductor and the metals across the interface. The main conclusions from impedance measurements are that the four-terminal data values mainly depend upon the bulk component of the ceramic and this held for all the spinel compositions studied herein despite the fairly low densities. This also indicates that the change in slope is unlikely to arise from microstructural features and instead may relate to phase or minor oxygen content changes (Fig. 7).

The spinel $MnFeCrO_4$ presents two linear regions with activation energies 0.573 and 0.835 eV below and above 290 °C. Sakai et al. [18] concludes that the iron component migrates to the surface at 800 °C and the iron content in $MnFe_xCr_{2-x}O_4$ has an important influence for the oxygen

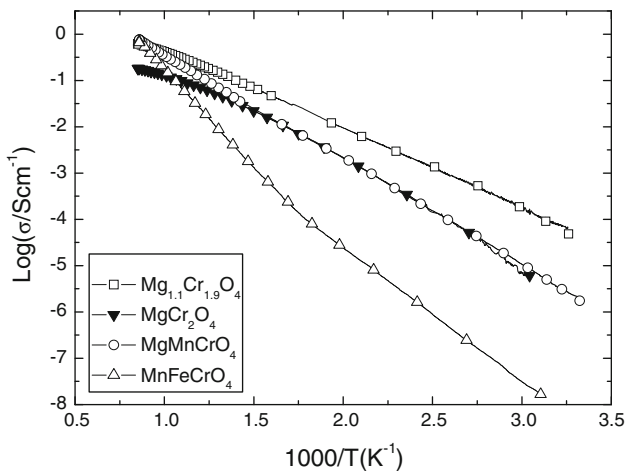

Fig. 7 The evolution of the conductivity versus temperature for spinels $Mg_{1.1}Cr_{1.9}O_4$, $MgCr_2O_4$, $MnFeCrO_4$ and $MgMnCrO_4$ in air between 100 and 900 °C

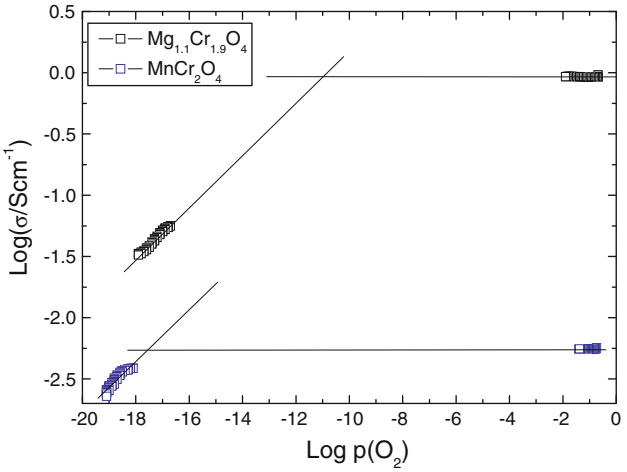

Fig. 8 Evolution of electrical conductivity versus partial pressure of the oxygen at 900 °C; guide lines show regions at $p(O_2)$ independent and (log σ/log $p(O_2)$) = 1/4 behaviour

content. A higher content of iron near the surface favours a higher diffusivity of the oxygen. The change of slope at 290 °C may relate to a change from grain boundary to bulk limited domination of conductivity. The same behaviour is observed for material $MgCr_2O_4$ with activation energies of 0.454 and 0.274 eV below and, respectively, above 370 °C. The spinel $MgMnCrO_4$ has a linear dependence of conductivity upon inverse temperature, with activation energy 0.447 eV and similarly $Mg_{1.1}Cr_{1.9}O_4$ has activation energy 0.321 eV. The Arrhenius plots for $Mg_{1.1}Cr_{1.9}O_4$ and $MgCr_2O_4$ have similar activation energies 0.447 and 0.454 eV above 370 °C.

Figure 8 presents only the apparently equilibrated data for conductivity of $MnCr_2O_4$ and $Mg_{1.1}Cr_{1.9}O_4$ as a function of oxygen partial pressure. The electrical conductivity decreases with the decrease of partial pressure of the oxygen (pO_2) for the considered spinels. This demonstrates p-type conductivity with an approximate $p(O_2)^{1/4}$ dependence, typical of many oxide semiconductors.

Discussion

X-ray diffraction results indicated the existence of one cubic phase for all as-prepared spinels. The XRD analysis for $Mn_{1.7}Cr_{1.3}O_4$, $Mn_{1.5}Cr_{1.5}O_4$ and $MgMnCrO_4$ showed the formation of a secondary phase after reducing the samples. The formed secondary phase was identified as cubic MnO. For spinels $MnFeCrO_4$ and $MnFe_{0.1}Cr_{1.9}O_4$, the formed secondary phases are MnO and metallic Fe. SEM studies confirmed the formation of secondary phases and that the amount of secondary phases increases with the reducing time. The observed SEM images show porous samples, with crystalline particles and a poor sinterability.

The compositions studied in reducing atmospheres showed p-type semiconducting behaviour with values of the order of 10^{-1} S cm^{-1}, at 900 °C. The electrical conductivity of the $Mn_{1+x}Cr_{2-x}O_4$ spinels increases with the manganese content, as observed for the studied compositions $x = 0$, 0.5. The conductivity value obtained for $Mn_{1.5}Cr_{1.5}O_4$ is about one order of magnitude higher than for $MnCr_2O_4$. The charge carrier flow might be due to electron hopping between Mn^{2+} at A-sites and Mn^{3+} at B-site and the difficulty of this electron transfer between A-sites determine the low conductivity and high activation energy. A higher content of manganese gives an improved conductivity for the material, due to electron transfer between Mn^{2+} and Mn^{3+} at B-site. $MgMnCrO_4$ spinel presents an increase of two orders of magnitude in electrical conductivity ($\sim$0.75 S cm^{-1}/900 °C), with occupation of A-sites with Mg^{2+} cations and Mn cations on B-sites, but the sample is not stable in reducing atmosphere, with formation of MnO as secondary phase.

The electrical conductivity for $MnFe_{0.1}Cr_{1.9}O_4$ should be higher than the one of $MnCr_2O_4$ due to the existence of cations with multiple oxidation states on B-site, but it is slightly smaller. The activation energy of $MnFe_{0.1}Cr_{1.9}O_4$ is higher than for $MnCr_2O_4$ and these results indicate that Fe can substitute both Mn at A-site and Cr at B-site in the spinel structure. For the sample $MnFeCrO_4$, the electrical conductivity is much higher, $\sim$0.7 S cm^{-1}/900 °C in air, as shown in Fig. 7. The conductivity might be improved by electron hopping between Fe^{2+} and Fe^{3+} ion on the B-site [18].

$MgCr_2O_4$ and $Mg_{1.1}Cr_{1.9}O_4$ show electrical conductivity values of $\sim$0.18 and 0.61 S cm^{-1} at 900 °C and also are stable in reducing atmosphere. It is suggested that Cr vacancies might form in this compound that favouring the p-type conduction by electron holes [21].

Conclusions

Two compositions important for further studies were found in the spinels $MgCr_2O_4$ and $Mg_{1.1}Cr_{1.9}O_4$. These compositions show stability in reducing atmosphere and an improvement in conductivity, considering the starting spinel composition studied, $MnCr_2O_4$, which only has conductivity of $\sim$0.005 S cm^{-1} at 900 °C in air. The electrical properties and TECs measured indicate that the best candidate for electrode support material is $Mg_{1.1}Cr_{1.9}O_4$. $MgMnCrO_4$ and $MnFeCrO_4$ also have good electrical conductivities. Their disadvantage is the instability in reducing atmosphere.

Acknowledgement The authors would like to express their gratitude to the Office of Naval Research for financial support.

References

1. Li Y, Wu J, Johnson C, Gemmen R, Scott X, Liu X (2009) Int J Hydrogen Energy 34(3):1489
2. Minh NQ, Takahashi T (1995) Science and technology of ceramic fuel cells. Elsevier Science, Amsterdam, The Netherlands
3. Chen X, Hou PY, Jacobson CP, Visco SJ, De Jonghe LT (2005) Solid State Ion 176:425
4. Konysheva E, Laatsch J, Wessel E, Tietz F, Christiansen N, Singheiser L, Hilpert K (2006) Solid State Ion 177:923
5. Krumpelt M, Cruse TA, Ingram BJ, Routbort JL, Wang S, Salvador PA, Chen G (2010) J Electrochem Soc 157(2):B228
6. Qu W, Jian L, Hill JM, Ivey DG (2006) J Power Sources 153:114
7. Yunus SM, Yamauchi H, Zakaria AKM, Igawa N, Hoshikawa A, Ishii Y (2008) J Alloys Compd 454:10
8. Kovtunenko PV (1997) Glass Ceram 54(5):9
9. Yang Z, Xia G, Simner SP, Stevenson JW (2005) J Electrochem Soc 152:A1896
10. Larring Y, Norby T (2000) J Electrochem Soc 147:3251
11. Choi JJ, Ryu J, Hahn BD, Yoon WH, Lee BK, Park DS (2009) J Mater Sci 44:843. doi:10.1007/s10853-008-3132-x
12. Petric A, Ling H (2007) J Am Ceram Soc 90(5):1515
13. Shannon RD (1976) Acta Cryst A32:751
14. Suzuki T, Adachi K, Katsufuji T (2007) J Magn Magn Mater 310:780
15. Yunus SM, Shim H-S, Lee C-H, Asgar MA, Ahmed FU, Zakaria AKM (2002) J Magn Magn Mater 241:40
16. Yakabe H, Baba Y, Sakurai T, Yoshitaka Y (2004) J Power Sources 135:9
17. Lu Z, Zhu J (2005) J Am Ceram Soc 88(4):1050
18. Sakai N, Horita T, Xiong YP, Yamaji K, Kishimoto H, Brito ME, Yokokawa H, Maruyama T (2005) Solid State Ion 176:681
19. Irvine JTS, Sinclair DC, West AR (1990) Adv Mater 2(3):132
20. Irvine JTS, Huanosta A, Valenzuela R, West AR (1990) J Am Ceram Soc 73(3):729
21. Moriwake H, Tanaka I, Oba F, Koyama Y, Adachi H (2002) Phys Rev B 65:153103